# THEORY AND OBSERVATION OF ANISOTROPIC AND EPISODIC INTERNAL WAVE EFFECTS ON 100-400 HZ SOUND

Timothy F. Duda[a],

[a]Applied Ocean Physics and Engineering Dept. Woods Hole Oceanographic Institution

Timothy F. Duda, WHOI AOPE Dept. MS 11, Woods Hole, MA 02543 USA. Fax 1 508 457 2104. Email: tduda@whoi.edu

***Abstract:*** *Propagation of sound through shallow-water internal waves of various types is discussed. The anisotropy of the waves imparts an anisotropy to their effects on sound. The internal waves are of two types: Long-wavelength internal tides and short-wavelength high-frequency waves. On the continental shelf both types of waves tend to move shoreward from deep water (i.e. have anisotropic motion and anisotropic correlation scales). The internal tides are less predictable than the surface tides that generate them. The short-wavelength nonlinear internal waves are also somewhat unpredictable, and also have anisotropic correlation scales, having crests of tens of kilometres in length but wavelengths of order 300 to 1000 m. Coupled-mode propagation dominates across-shelf sound propagation, which in the direction of short internal wave correlation scale. Refracted-mode propagation dominates along-shelf propagation. Data from two sea exercises illustrate the character of the waves and their effects on sound.*

***Keywords:*** *Internal waves, nonlinear internal waves, internal tides, coherence, shallow-water acoustics.*

## 1. INTRODUCTION: INTERNAL WAVES IN SHALLOW WATER

Internal waves in the coastal ocean are one of the dominant causes of spatial and temporal sound-speed variability. They occupy the horizontal wavelength domain of hundreds of meters to tens of kilometres, and have time scales of tens of minutes to one day. The detailed behaviour of individual waves is modulated over time by processes with larger length scales and longer time scales than the waves themselves.

On the outer portion of many continental shelves the internal waves are directly related to the tides. The internal tides (internal waves of tidal frequency) that appear are the result of vertical deflection of tidal currents by sloping bathymetry. In the presence of a local vertical potential density gradient, the vertical motions create periodic internal density anomalies and pressure anomalies that lead to radiation of internal gravity waves [1]. The wavelengths of these waves are typically near 50 km for semidiurnal constituents (two periods per day), and near 100 km for diurnal constituents. Because the lower bound of internal wave frequencies is the inertial frequency, two times the rotation rate of earth times the sine of latitude, there are no diurnal internal tides at latitudes above 30° N or S.

Internal tides can form at the continental slope, just offshore of the outer continental shelf. The continental slope is an anisotropic feature. Internal tides generally propagate offshore and onshore, in somewhat of a plane-wave fashion. The waves directed toward shallow water show increasing energy density over time (disregarding dissipation), and can evolve into packets of short and steep nonlinear internal waves with wavelengths of order one km or less. This is consistent with the nonlinear nature of the Navier-Stokes equations [1]. Fig. 1 schematically shows crests of nonlinear packets moving onshore, drawn for shelf-edge areas of two joint internal-wave/acoustics field programs. Fig. 1 also shows two incident transbasin nonlinear internal waves, waves of a different type [2].

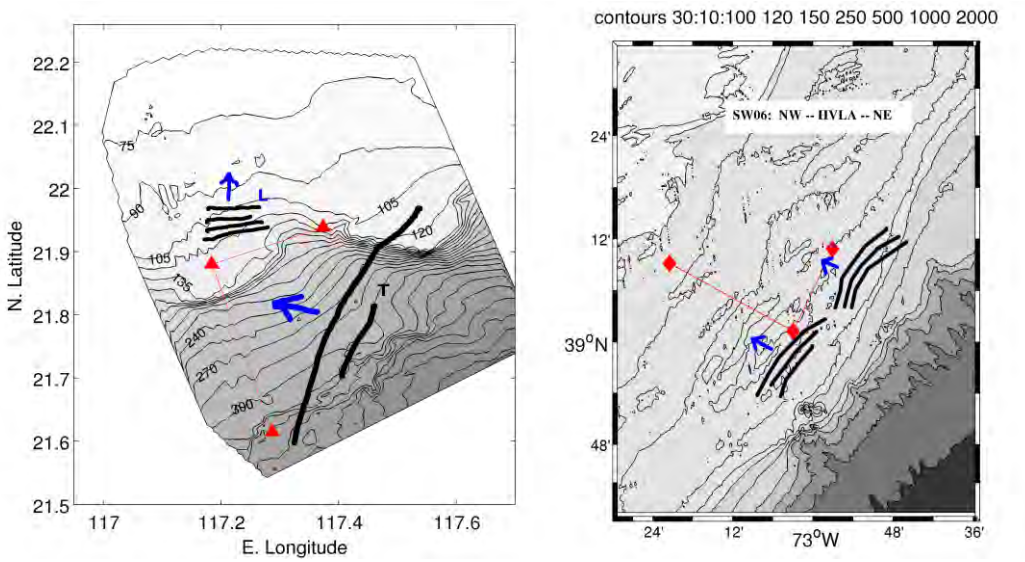


*Fig.1: (left) The ASIAEX 2001 South China Sea source and receiver positions are shown, with the receiver at the vertex. Crests of example nonlinear internal wave of two types are drawn, waves locally generated from the internal tide (L), and transbasin type waves (T). (right) The Shallow-Water 2006 program source and receiver positions are shown, again with the receiver at the vertex. Example locally generated nonlinear wave crests are drawn. Depth contours in meters.*

## 2. ACOUSTICALLY RELEVANT WAVE FEATURES

The internal waves cause large transient displacements of the thermocline, which have a one-to-one correspondence with sound-speed anomalies. Many recent papers discuss the effects of these anomalies on sound propagation. In many areas the waves travel on a thermocline that (typically) separates a warm thin upper later from underlying cool water. The long internal tides have approximately sinusoidal displacements at a given depth. The short nonlinear waves are unidirectional in displacement, directed away from the thin layer (typically down, drawing warm water downward, giving fast sound-speed anomalies). Here we focus on the anisotropic nature of the effects, and the fact that that packets of large waves often appear at a given location only once per tidal cycle, with minor wave activity between the packets. There are many exceptions to this rule, often caused by waves arriving from more than one source region, with source regions apparently spread along the spatially varying shelf break. Details of internal tide generation processes and nonlinear wave development processes as they occur in the field are not well known.

The schematic internal-wave crests drawn in Fig. 1 have many features drawn from airborne synthetic aperture radar (SAR) images, satellite SAR images, and other shipboard or moored observations [3]. The internal tides have very long wavelength, and lose much of their energy to nonlinear waves and/or dissipate that energy within one-half wave period (wave length) of being generated. As a result, their sound-speed anomalies are weakly anisotropic compared to those of the nonlinear waves. The nonlinear waves have long crests compared to their wavelengths, with aspect ratios of 10 to 1 or more, but the curved nature of the wave packets [4] has a reducing effect on objective measures of the sound-speed perturbation field anisotropy.

The anisotropy of the sound-speed perturbation field imparts anisotropy to anomalous sound propagation effects, also known as forward scattering effects. Propagation normal to the internal wave crests (at 90°) is subject to coupled normal-mode propagation [5]. Propagation aligned with the wave crests is subject to horizontal refraction of normal modes [6], with mode coupling being weak or nonexistent, so-called adiabatic normal mode propagation. At in-between angles there may be a gap between the two behaviours, but there has been some evidence that mode coupling can occur for angles of order 8°, so there would be no gap. The existence of the gap may depend on ambient conditions and wave characteristics of each area under consideration.

## 3. TEMPORAL VARIATIONS OF INTENSITY

There have been a few theoretical studies of the effects of anisotropic internal waves on sound intensity. Coupled-mode studies of sound normal to crests show that short moving internal waves cause alternating net mode coupling into mixtures of modes that are more attenuated (highly bottom interacting) or less attenuated, respectively. The effects of this on intensity are tied to range travelled *after* the coupling event at the wave packet, and reach order 10 dB at order 30 km, with a strong dependence of this rule on seafloor type, thermocline conditions, and acoustic frequency. Sound travelling along the crests of the waves is subject to many refractive effects in the horizontal [4]. Phase velocity anomalies of normal modes can grow large in the waves, with duct critical angles of 3° or 4°, creating mode multipath (modal interference patterns) and mode shadow zones. These

effects can be modelled and understood using the adiabatic mode approximation. The effects also exist in the presence of mode coupling. Because they depend on modal phase, mode coupling effects have strong temporal variability, and the mixed situation will reflect the temporal variations of the mode coupling as well as that of the (possibly) evolving refraction geometry.

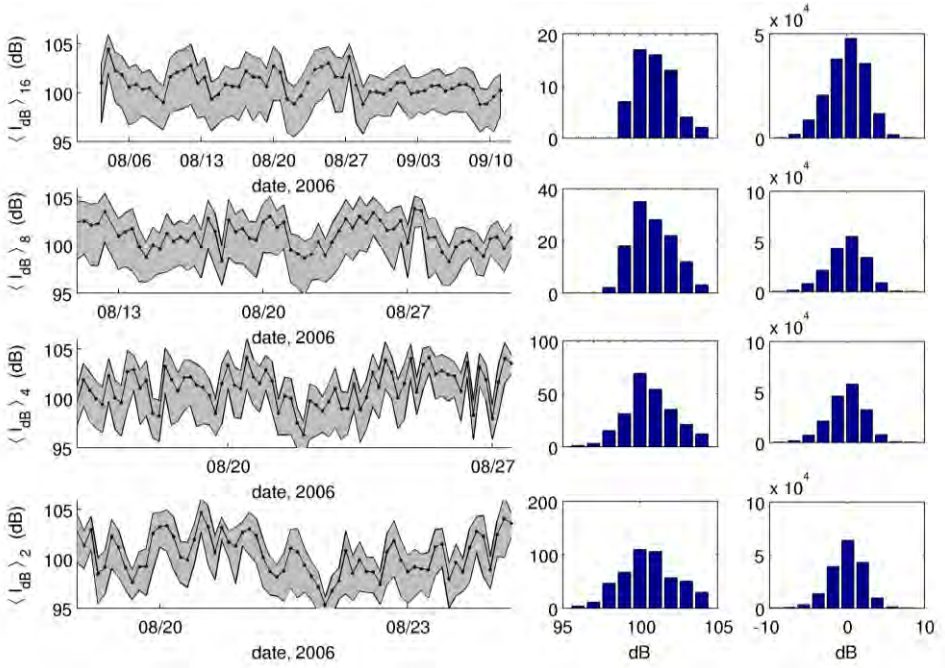


*Fig 2: SW06 VLA channel 10 receptions of the 224-Hz pulse arrivals. Left, from top to bottom, are mean pulse intensities E in windows of 16, 8, 4, and 2 hrs, +/- standard deviation of residuals for the windows. The time scales are stretched so that the bin quantities in the plots are equal. The middle column shows histograms of E. The right column shows histograms of the residuals.*

The fluctuation levels are demonstrated with data from two experiments drawn in Fig. 1., the 2001 ASIAEX study in the South China Sea, and the Shallow-Water 2006 study south of New York. The details of the acoustic experiments can be found in reports [7,8]. Fig. 2 shows time-averaged receptions of sound at a mid-depth phone of the SW06 HVLA receiving array (southernmost symbol in Fig. 1). Sound is from a 224-Hz source 30 km to the northwest at station NW. Sound propagation was across internal wave crests. Intensity averaged over dispersed pulse duration and over lengthy time windows (many pulses) is shown for four window sizes, ranging from 2 to 16 hours. This gives the frequency content of the fluctuations. The analysis is performed this way because the transmission schedule was irregular, with large gaps. The pattern of intensity versus time that appear when the averaged results are viewed in bin-width normalized time, as in the plot, are rather similar for all window lengths, suggesting self-similarity. The fractal (Hausdorff) dimension for the intensity pattern is $D$ = 2.5-0.5β, where β is the downward power spectral slope [9]. Using special methods to compute the power spectrum of the unequally spaced data, Fig. 3 (left) shows β to be −0.5 for the 224-Hz data, for 200-Hz pulses from the NE SW06 path, and for ASIAEX pulses from the shallow source (Fig. 1). This shallow spectral slope gives the large value $D$ = 2.25. The shallow spectral slope results in a high level of high-frequency intensity variations, middle panel of Fig 3. This is consistent with studies of effects of moving internal waves made by our group and by others.

Despite the anisotropy of the internal waves there are only negligible differences in the intensity spectra for the two SW06 paths. Anisotropy does appear in the 2-hr binned intensity, however. Fig. 3 shows histograms of sound for the across-crest (224 Hz) and along crest (200 Hz) paths. The across-crest statistics are closer to normal than the along-crest statistics, which show skewness (a high number of low intensities). The skewness is consistent with shadow zones predicted for paths nearly aligned with crests [4]. Finally, for the NW (across-crest) case, modelling shows that time-dependence of the relative excitation of the normal modes as wave pass the source can only give a few dB variation at tens of km, compared to the 10 dB or greater coupling-induced intensity changes.

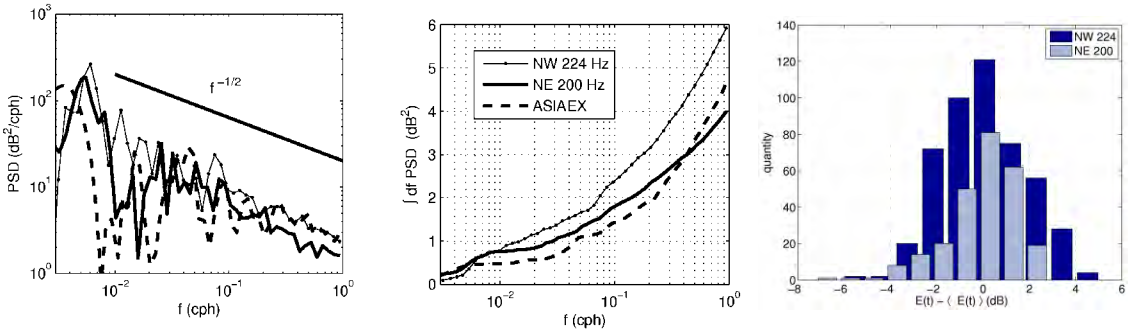


*Fig. 3: (left) The power spectra of single-point intensities for three propagation paths are shown. The legend is in the center. (center) Integrated spectra (cumulative variance). (right) Histograms of 2-hour averaged intensity, two sources.*

## 4. HORIZONTAL COHERENCE

The horizontal coherence length is of interest because it determines the limiting useful length of horizontal arrays. Gain in signal to noise ratio can be obtained only for signals that are phase coherent over the array. The correlation scale was measured in detail during the SW06 program. Pulses of 100 and 200 Hz center frequency were transmitted 19.5 km from the NE station, and pulses of 224 and 400 Hz were transmitted 30 km from the NW station. Measurements along a northward-directed bottom-resting 32-element array (the horiz. line array, HLA) with 15-m spacing were analyzed. Many statistics of the complex-demodulated fields were computed for the duration of the one-month experiment, each as a function of beam steering angle. These included array gain for apertures of 2, 4, 8, 16 and 32 contiguous hydrophones, phase structure function, and spatially lagged correlation function. Further details are available elsewhere [8,10]. The normalized lagged covariance (cross-correlation) function is presented here, defined as

$$R_N(x) = \frac{\left\langle \Psi^*(x_0)\Psi(x_0+x)\right\rangle}{\left\langle \Psi(x_0)^2\right\rangle^{1/2}\left\langle \Psi(x_0+x)^2\right\rangle^{1/2}}\ ; \qquad R_N(0)=1 \tag{1}$$

The angle brackets indicate an average over time. Here, 2.4-hr windows are used (10 windows per day).

Functions $R_N(x)$ are plotted for NW 224-Hz pulses at the top of Fig. 4. These have a remarkably steady behaviour, with correlation lengths $L$ ($1/e$ scales of $R_N$) staying near 12 wavelengths. Behaviour at 400-Hz is similar. The steady-state correlation length is consistent with coupled-mode propagation and one or more internal-wave packets between

the source and receiver. On the other hand, the $L$ scales are much shorter than predicted from a coupled analytic/computational study. One candidate explanation for this is that one end of the array is closer to the source than the other, and mode interference is variable across the HLA. The maximum $L$ expected in this geometry can be computed using a joint horizontal/vertical array processing method [10]. This maximum would occur for HLA sampling of plane-wave arrival of modes detected at the VLA moored at one end of the HLA. The observed $L$ are always lower than this maximum, suggesting strong azimuthal variations in the propagation of sound fields from the point source.

The same functions are shown for the along-crest 200-Hz pulses arriving from NE (Fig. 4, lower panel). The correlation length $L$, again given by the $1/e$ contour, fluctuates dramatically as packets of waves with crests that are approximately aligned with the sound path intrude. The wave arrivals can be seen at the top edge of the lower panel of Fig. 4. The behavior is consistent with refraction of modes, which has been analyzed in a few recent papers [e.g. 11]. Effects such as crossing distinct arrivals of each mode are possible, which give strong fluctuations of amplitude and phase (interference pattern). Phase decorrelation has been identified as the primary cause of reduced coherence.

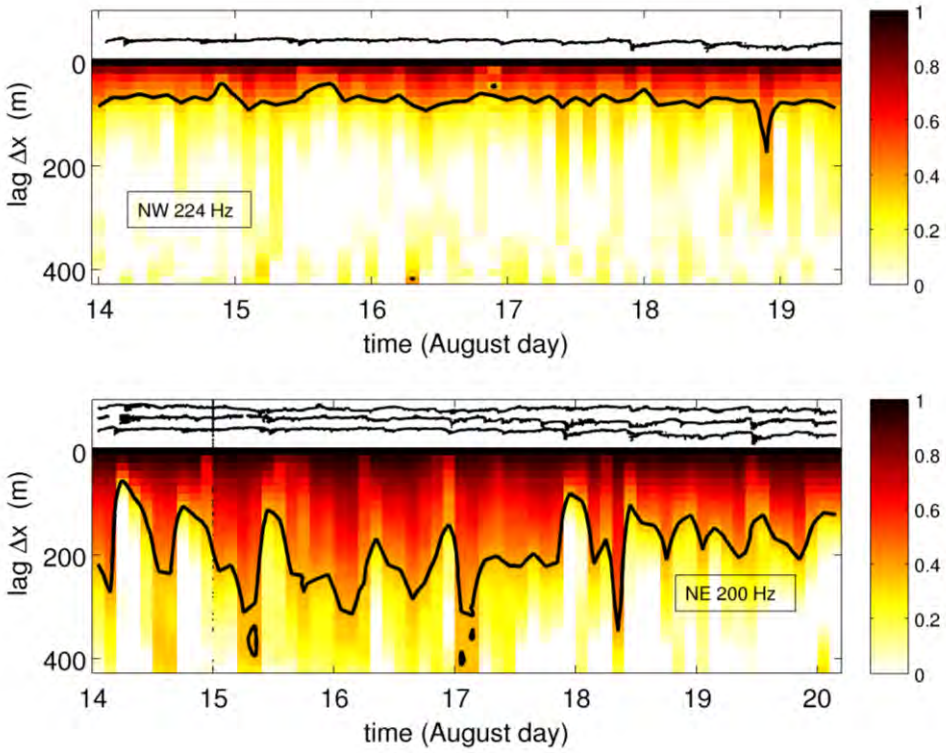


*Fig. 4: Horizontal correlation functions are plotted for 200-Hz pulses transmitted 20 km along-shelf in SW06 (bottom), and 224-Hz pulses transmitted 30-km across-shelf (top). 2.4-hour averaging windows are used. The lines show the 1/e contours. (upper section, lower panel) 15 ° Isotherm displacements (m) are shown at the receiver location, a mid point, and the source location northeast of the receiver (bottom to top). The displacements at the receiver are repeated in the upper section of the top panel.*

Array performance analysis has been used as a motivation for studying the horizontal correlation. Theoretical signal to noise ratio gain for $M$ hydrophones over one hydrophone is given by $G$=10log10($M$) if noise is uncorrelated between phones and signal is correlated at all phones, with $G$ in dB. Array gain degradation is $AGD.M=G(M)-G_F(M)$, where $G_F$ is

gain obtained in the field. Fig. 5 shows 32-element and 4-element degradation on a pulse-by pulse basis for 2.4 hours and for NE 100-Hz data. White on the two top panels shows AGD.32 or AGD.4 equal to zero, or good gain, and dark colors are poor gain. There are strong variations over time at the angle directed at the source (~27°) as internal waves pass in this early part of Aug 14 (see Fig. 4). The theoretical gain ($G$) is 15 dB for $M$=32, and 6 dB for $M$=4. Fig. 5c shows gain averaged over the 2.4 hours for (from bottom at 28 degrees) $M$=1,2,4,8,16,32. Gain for all $M$ =32 is far below theoretical.

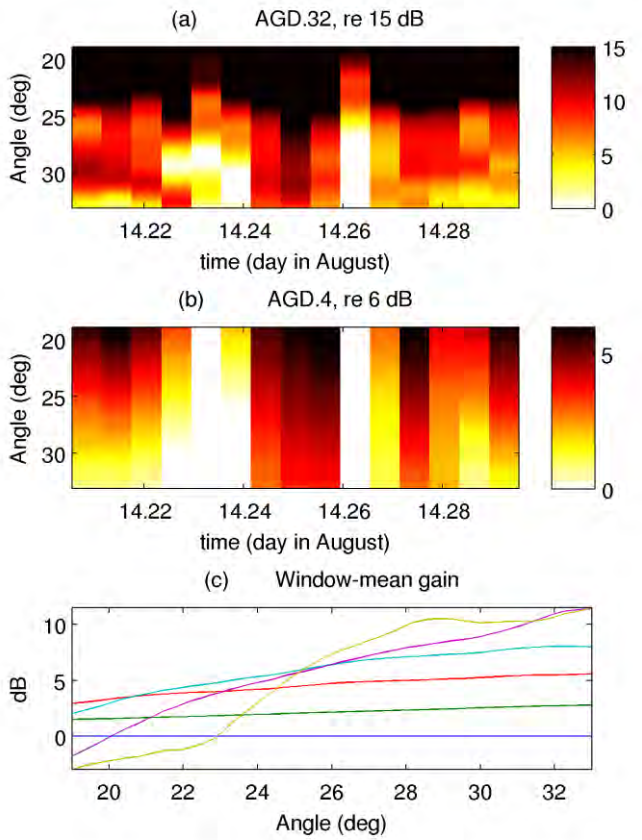


*Fig. 5: (a) Array gain degradation for the full array, 32 elements, as a function of steering angle and time. (b) Same as (a), except for 4-elements subarrays. Subarray averaging is used to improve reliability of statistics. (c) Averages of $G_F$ over the 2.4 hour time window (day 14.2 to 14.3) for each angle are shown.*

## 5. SUMMARY

Data from the SW06 experiment south of New York, USA, has been used to compare characteristics of pulses propagated along paths aligned and normal to the nominal geometry of internal wave crests. The high-degree of anisotropy in the internal waves causes high anisotropy in field correlation statistics measured with a horizontal line array. Temporal fluctuations of intensity have some statistics that appear independent of angle (i.e. isotropic), but also display some anisotropic features. Theories of refracted normal-mode propagation can be used to predict the nature of the statistical variations. It is likely that characteristics of internal waves and wave packets may need to be known in detail to sufficiently predict correlation and array gain behaviour. Some of these characteristics are not yet well known, such as variations of along-crest structures and curvatures in internal

waves at a single site, or variations between sites. Further research into these variations and their causes may improve this situation.

## 6. ACKNOWLEDGEMENTS

The efforts of James Lynch, Steve Ramp, and David Tang as lead PI's of ASIAEX South China Sea are appreciated, as well as Lynch's effort as lead PI of SW06. Efforts of all technical staff and marine staff are appreciated. Funding for this work is from the Office of Naval Research, Ocean Acoustics Program.

## REFERENCES

[1] **Vlasenko, V., N. Stashchuk, and K. Hutter**, *Baroclinic Tides*, Cambridge U. P., 351 pp., 2005

[2] **Duda, T. F., J. F. Lynch, J. D. Irish, R. C. Beardsley, S. R. Ramp, C.-S. Chiu, T. Y. Tang and Y. J. Yang,** Internal tide and nonlinear internal wave behavior at the continental slope in the northern South China Sea, *IEEE J. Oceanic Eng.,* 29, 1105-1130, 2004

[3] **Jackson, C. R.,** *An Atlas of Internal Solitary-Like Waves and Their Properties, 2nd ed.* Global Ocean Associates, Alexandria, VA, 2004. Available at http://www.internalwave atlas.com/Atlas2_index.html.

[4] **Lynch, J. F., Y.-T. Lin, T. F. Duda and A. E. Newhall,** Acoustic ducting, reflection, refraction, and dispersion by curved nonlinear internal waves in shallow water, *IEEE J. Oceanic Eng*., 35, 12-27, 2010.

[5] **Preisig, J. C., and T. F. Duda,** Coupled acoustic mode propagation through continental-shelf internal solitary waves, *IEEE J. Oceanic Eng,* 22, 256-269, 1997.

[6] **Katsnel'son, B. G., and S. A. Pereselkov,** Low-frequency horizontal acoustic refraction caused by internal wave solitons in a shallow sea, *Acoust. Phys*., 46, 684–691, 2000.

[7] **Newhall, A., L. Costello, T. Duda, J. Dunn, G. Gawarkiewicz, J. Irish, J. Kemp, N. McPhee, S. Liberatore, J. Lynch, W. Ostrom, T. Schroeder, R. Trask, and K. Von der Heydt,** Preliminary acoustic and oceanographic observations from the ASIA-EX 2001 South China Sea Experiment, WHOI Tech. Rept., WHOI-2001-12, 2001.

[8] **Newhall, A. E., T. F. Duda, K. von der Heydt, J. D. Irish, J. N. Kemp. S. A. Lerner, S. P. Liberatore, Y.-T. Lin, J. F. Lynch, A. R. Maffei, A. K. Morozov, A. Shmelev, C. J. Sellers, W. E. Witzell,** Acoustic and oceanographic observations and configuration information for the WHOI moorings from the SW06 experiment, Woods Hole Oceanographic Institution Technical Report, WHOI-2007-04, 2007.

[9] **Churnside, J. H. and J. J. Wilson,** Power spectrum and fractal dimension of laser backscattering from the ocean, *J. Opt. Soc. Am. A.,* 23, 2829-2833, 2006.

[10] **Collis, J. M., T. F. Duda, J. F. Lynch, and H. A. Deferrari,** Observed limiting cases of horizontal field coherence and array performance in a time-varying internal wavefield, *J. Acoust. Soc. Am*., 124, EL97-EL103, 2008**.**

[11] **Badiey, M., B. G. Katsnelson, J. F. Lynch, and S. Pereselkov,** Frequency de-pendence and intensity fluctuations due to shallow water internal waves, *J. Acoust. Soc. Am.,* 122, 747–760, 2007